Applied Physics Letters

High performance InGaAs/GaAsSb terahertz quantum cascade lasers operating up to 142 K

Cite as: Appl. Phys. Lett. **101**, 211117 (2012); https://doi.org/10.1063/1.4766915
Submitted: 01 October 2012 • Accepted: 26 October 2012 • Published Online: 21 November 2012

C. Deutsch, M. Krall, M. Brandstetter, et al.

AIP Publishing

High performance InGaAs/GaAsSb terahertz quantum cascade lasers operating up to 142 K

C. Deutsch,[1,a)] M. Krall,[1] M. Brandstetter,[1] H. Detz,[2] A. M. Andrews,[2] P. Klang,[2] W. Schrenk,[2] G. Strasser,[2] and K. Unterrainer[1]
[1]*Photonics Institute and Center for Micro- and Nanostructures, Technische Universität Wien, Gusshausstrasse 27-29, 1040 Vienna, Austria*
[2]*Institute for Solid State Electronics and Center for Micro- and Nanostructures, Technische Universität Wien, Floragasse 7, 1040 Vienna, Austria*

(Received 1 October 2012; accepted 26 October 2012; published online 21 November 2012)

We report on the demonstration of a maximum operating temperature of 142 K for InGaAs-based terahertz quantum cascade lasers. This result is achieved by using the alternative material combination $In_{0.53}Ga_{0.47}As/GaAs_{0.51}Sb_{0.49}$, lattice-matched to InP, which exhibits fabrication advantages over standard $In_{0.53}Ga_{0.47}As/In_{0.52}Al_{0.48}As$ due to more suitable material parameters. An active region, based on a three-well phonon depletion design, with improved injection and extraction tunneling coupling, was designed. The devices exhibit threshold current densities of 0.75 kA/cm^2 and provide peak optical powers up to 9 mW. A broad spectral emission range between 3.3 and 4 THz is measured.
 [http://dx.doi.org/10.1063/1.4766915]

Quantum cascade lasers (QCLs) are tailor-made semiconductor heterostructures[1] and currently able to cover the mid-infrared (3–25 μm) and terahertz (60–250 μm) spectral range.[2,3] In principle, QCLs could be realized in various semiconductor material combinations due to band structure engineering. However, designers of mid-infrared and terahertz (THz) QCLs have different preferred material combinations. Mid-infrared QCLs show unprecedented device performance using InP-based InGaAs/InAlAs,[4] whereas THz QCL performance records are demonstrated using $GaAs/Al_{0.15}Ga_{0.85}As$.[5,6] A large refractive index difference between the InP substrate and the InGaAs/InAlAs active region has advantages for mid-infrared waveguide fabrication. In addition, the InGaAs effective electron mass ($m^* = 0.043m_0$ when lattice-matched) is about one third lower than in GaAs ($m^* = 0.067m_0$). Since the gain scales with $m^{*-3/2}$, InGaAs can produce twice as high optical gain as GaAs.[7] Consequently, this raises the question why THz QCLs are yet almost exclusively fabricated with GaAs/AlGaAs and only a few attempts have been made using InGaAs/InAlAs.[8–10] Up to now, the maximum operating temperature of 122 K for InGaAs/InAlAs is considerably lower than for GaAs/AlGaAs.[5,9]

Growth quality is one of the most restricting criteria when it comes to the realization of QCL active regions in any material system. It is also the main reason why the temperature record of 200 K in THz QCLs is still held by the GaAs/AlGaAs material system.[5] Another example of the importance of growth quality is short wavelength QCLs.[11] Despite the material parameter advantages of InAs/AlSb, like the extremely low InAs effective electron mass combined with a high conduction band offset and the absence of alloy scattering in the well, the mature growth of InP-based InGaAs/InAlAs, even when highly strained, enables the performance records at 3.4 μm.[12]

Recently we have demonstrated THz QCLs in the InP lattice-matched $In_{0.53}Ga_{0.47}As/GaAs_{0.51}Sb_{0.49}$ material system.[13] The replacement of InAlAs with GaAsSb barriers targets the main disadvantage of $In_{0.53}Ga_{0.47}As/In_{0.52}Al_{0.48}As$ over $GaAs/Al_{0.15}Ga_{0.85}As$, which is the high conduction band discontinuity of 520 meV instead of ~120–150 meV. For active regions in THz QCLs, this results in ultrathin barrier layers down to the monolayer level[8] and hence high demands on the growth thickness accuracy or the use of robust designs.[14] GaAsSb barriers offer several advantages to relax these restrictions on the growth: The conduction band offset is reduced to 360 meV, it has a lower effective electron mass of $0.045m_0$ and the heterostructure alignment is type II.[15] These material properties make the electron barrier more penetrable, and therefore thicker barrier layers can be employed in the active region design.[13]

To illustrate the influence of such material parameters on the layer thicknesses, we designed the injector part of a typical three well phonon depletion active region, using four different material systems: $GaAs/Al_{0.15}Ga_{0.85}As$, $In_{0.53}Ga_{0.47}As/In_{0.52}Al_{0.48}As$, $In_{0.53}Ga_{0.47}As/GaAs_{0.51}Sb_{0.49}$ and $GaAs/Al_{0.40}Ga_{0.60}As$. The injector consists of two wells and the injection barrier, shown in Fig. 1. The band structures are calculated with a 1D effective mass Schrödinger solver and are plotted for an electric field, where the tunneling resonance between subbands 2 and 3 occurs. The width of the broad well is designed to meet the energy of the longitudinal optical (LO) phonon for efficient depletion in the particular material system, which is 36 meV for GaAs and 34 meV for InGaAs. The injector barrier is designed to give an anticrossing energy of 2.5 meV at resonance, which is close to the optimized values found in the best active region designs.[5,16] The subsequent well is designed to reach the alignment field (resonance between subbands 2 and 3) at the same voltage drop, independent of the material combination. The total voltage drop per period is almost entirely given by the emission frequency plus LO phonon resonance in a three-well design. Fig. 1(a) depicts the injector part for the commonly

a)Electronic mail: christoph.deutsch@tuwien.ac.at.

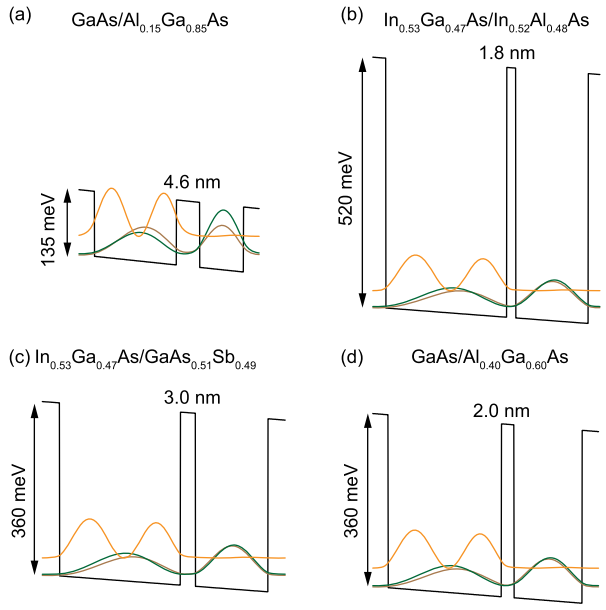

FIG. 1. Influence of different material system and their parameters on the injection barrier width in THz QCLs. The injector barrier is designed for an anticrossing energy of 2.5 meV at resonance. The comparison shows the drawback of the InGaAs/InAlAs material system as it requires the thinnest barrier, which sets narrow tolerances for growth accuracy. Replacing InAlAs with GaAsSb allows for a 67% thicker barrier and therefore relaxes the demands on the growth.

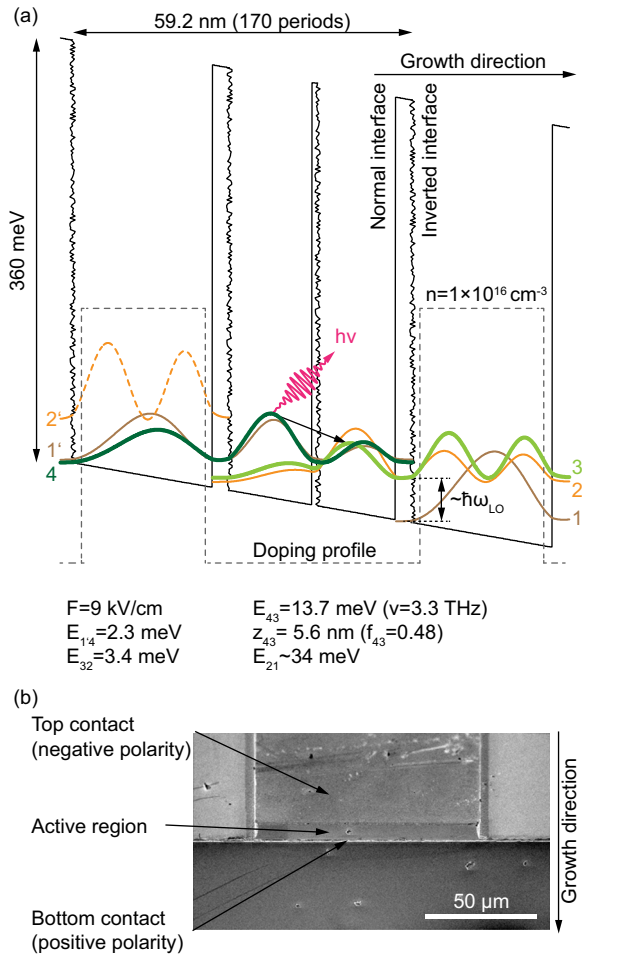

FIG. 2. (a) Band structure of a three-well phonon depletion active region designed in the lattice-matched $In_{0.53}Ga_{0.47}As/GaAs_{0.51}Sb_{0.49}$ material system. The band structure is shown at the injection resonance, occurring at an applied electric field of 9 kV/cm. The layer sequence in nanometers, starting from the widest well is 2.0/*20.3*/2.0/**3.0**/14.4/**1.0**/13.5/**3.0**, with barriers indicated in bold fonts and with the doped section italicized. The interface asymmetry of GaAsSb barriers, with respect to the growth direction, is sketched as a rough conduction band profile at the inverted interfaces. (b) Negative top contact polarity is applied to operate the devices in the reverse direction. The resulting electron transport in the growth direction, which is incident on the normal interfaces, avoids enhanced interface roughness scattering due to the aforementioned asymmetry for GaAsSb barriers.

used $GaAs/Al_{0.15}Ga_{0.85}As$ system with an injector barrier of 4.6 nm. Switching to the mid-infrared QCL materials choice $In_{0.53}Ga_{0.47}As/In_{0.52}Al_{0.48}As$ in Fig. 1(b) dramatically reduces the barrier thickness to 1.8 nm. The benefit of replacing InAlAs with GaAsSb can be seen in Fig. 1(c). Due to the aforementioned properties of GaAsSb, the barrier layer can be widened to 3 nm with yet using an InP-based heterostructure. In order to show that this is not only the effect of the reduced conduction band offset compared to InAlAs, we also compare it with $GaAs/Al_{0.40}Ga_{0.60}As$. $GaAs/Al_{0.40}Ga_{0.60}As$ and $In_{0.53}Ga_{0.47}As/GaAs_{0.51}Sb_{0.49}$ exhibit the same conduction band offset of 360 meV. However, for the Al containing material system the calculated barrier thickness is 2 nm. The difference can be attributed to the lower effective electron mass in the barrier and a strong nonparabolicity effect due to the type II heterostructure alignment in $In_{0.53}Ga_{0.47}As/GaAs_{0.51}Sb_{0.49}$.[13,17]

The previously demonstrated InGaAs/GaAsSb THz QCLs were not able to outperform the best InGaAs/InAlAs devices and suffered from a relatively high leakage current.[13] Fig. 2(a) shows the revised active region design, which is again based on a three-well phonon depletion scheme. The revised design employs thicker injector and extractor barriers, resulting in reduced tunneling couplings that are now closer to known optimized values. Anticrossing energies are now 2.4 and 3.5 meV for the injection and extraction path, respectively. The optical transition energy is designed to be 13.7 meV ($\nu = 3.3$ THz) with an oscillator strength of 0.48.

The growth order and the resulting operating direction in the presented devices is particularly important, as it plays a major role for the performance of THz QCLs.[18] Especially in the case of InGaAs/GaAsSb, a pronounced interface asymmetry due to the mixing of group V elements in the barrier material leads to significantly better device performance in the reverse operating direction.[19] The inverted interfaces (GaAsSb terminated) suffer from increased interface roughness, and hence the opposite (traditional) operating direction would lead to higher elastic interface roughness scattering, degrading the device performance in every aspect.[18] The interface asymmetry with respect to the growth direction is also illustrated in the conduction band profile in Fig. 2(a). The authors want to emphasize that previous InGaAs/GaAsSb THz QCLs have been operated in the reverse direction and that the performance improvements reported in this paper are mostly related to active region design changes. Fig. 2(b) shows the applied bias polarity with respect to the growth direction. Note that this is in contrast to the majority of published THz QCLs.

The sample was grown by solid-source molecular beam epitaxy and 170 repetitions of the module yield a total thickness

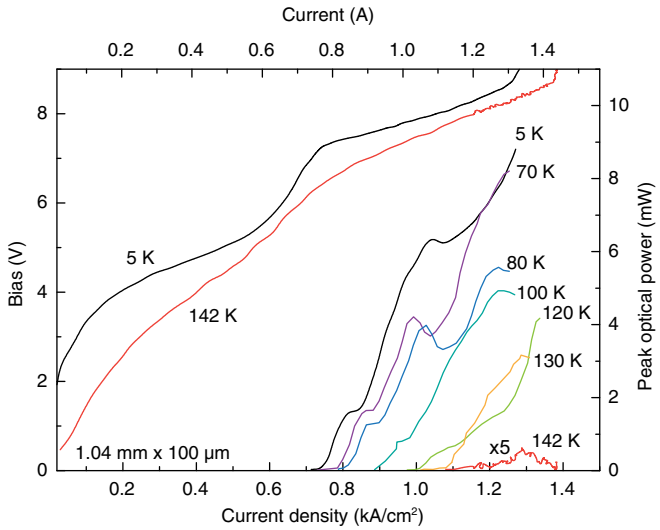

FIG. 3. Temperature-dependent light-current characteristics of a 1.04 mm $\times$ 100 μm double metal ridge operated in pulsed mode (150 ns, 25 kHz). The current-voltage curve is plotted at a heat sink temperature of 5 and 142 K. The threshold current density at 5 K is 0.75 kA/cm^{-1}, and the device works up to a maximum temperature of 142 K.

of 10 μm. 100 and 50 nm InGaAs contact layers, doped to 7×10^{18} cm^{-3}, were grown at the bottom and the top of the active region structure, respectively. Si doping was employed in the wide well with a bulk density of 1×10^{16} cm^{-3}, which translates into a sheet carrier density of 2×10^{10} cm^{-2} per module. The grown structure was processed into double metal ridge waveguides using Ti/Au metallization. The fabrication steps are almost identical to Ref. 13 with minor changes. The SiN etch protection mask was replaced by a self-aligned Ni mask. The Ni mask was deposited together with the top metallization and was removed after deep etching. An SEM picture of a fabricated device with cleaved facets, instead of lithographically

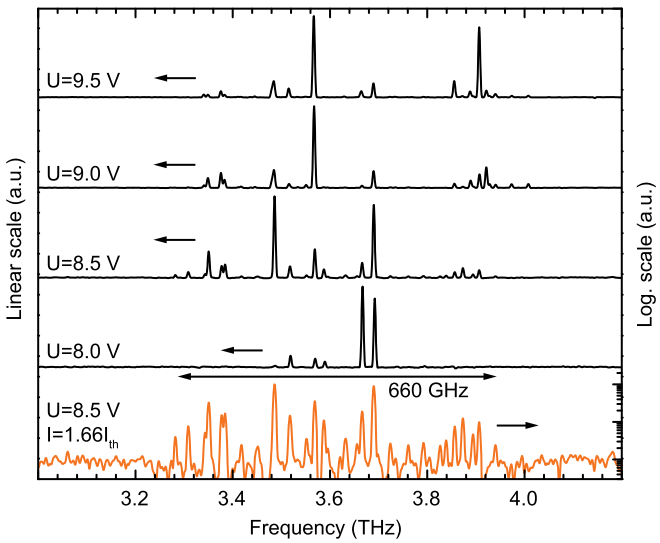

FIG. 4. Normalized spectra recorded at different bias voltages (pulsed mode 25 kHz, 300 ns) and at a heat-sink temperature of 5 K. The bandwidth of 660 GHz at 8.5 V is also plotted in logarithmic scale. This relatively broad bandwidth is attributed to enhanced interface roughness in the InGaAs/GaAsSb material system, which acts as a source for inhomogeneous broadening of the optical transition.

defined and etched facets used in the previous devices, is shown in Fig. 2(b).

The light-current-voltage (LIV) characteristic of a 1.04 mm long and 100 μm wide ridge is displayed in Fig. 3. The device was driven in pulse mode with a pulse duration of 150 ns and a repetition rate of 25 kHz. The revised barrier widths lead to a reduced parasitic leakage, and the threshold current density is 0.75 kA/cm^2. The maximum peak optical power of 9 mW was measured with a calibrated thermopile detector integrated within the cryostat to avoid water absorption. The active detector element has a diameter of 6 mm and was mounted at a distance of approximately 5 mm from the device facet. Temperature-dependent LI characteristics were recorded with a pyroelectric detector and are also shown in Fig. 3. The maximum operating temperature of the device is 142 K, which clearly outperforms the best InGaAs/InAlAs THz QCLs demonstrated so far, working up to 122 K.[9] A fit of the temperature dependent threshold current density with the commonly used formula $J_0 + J_1 \cdot \exp(T/T_0)$ reveals a characteristic temperature T_0 of 34 K.

Fig. 4 exhibits spectra recorded at different bias values and in pulsed mode (300 ns, 25 kHz). Spectra were recorded with a Bruker Vertex 80 Fourier transform infrared spectrometer and at a resolution of 0.125 cm^{-1}. The absolute bandwidth of 660 GHz at 8.5 V ($I = 1.66I_{threshold}$) is outstanding for a homogenous active region structure. The modes are centered around 3.6 THz, yielding a relative bandwidth of $\Delta f/f_0 \sim 18\%$. We attribute this broadband emission to the, compared to GaAs/AlGaAs structures, increased interfaces roughness which is inherent for As-Sb material systems.[19] Interface roughness in fact acts a source for inhomogeneous gain broadening in QCLs.[20]

In conclusion, we demonstrated high performance InGaAs-based THz QCLs operating up to a maximum heat-sink temperature of 142 K. The replacement of standard InAlAs barriers with GaAsSb, lattice-matched to InP, leads to a more attractive material system for the fabrication of THz QCLs. However, the question remains whether the material system is competitive with GaAs. GaAs/AlGaAs growth has reached an extreme degree of quality, and record-performing three-well active regions are probably perfectly optimized.[5] Nevertheless, the performance of InGaAs/GaAsSb THz QCLs can already keep up with state of the art GaAs/AlGaAs devices when taking into account the emitted bandwidth, and lower loss copper waveguides have not been employed in the presented devices.[14,21,22] The future potential definitely lies in further active region optimizations (subband alignment, oscillator strength, etc.) and in a better understanding/compensation of growth asymmetries,[18] eventually exploiting the full potential of the low effective electron mass in InGaAs.

The authors acknowledge the support by Austrian Scientific Fund FWF (SFB-IRON F25, DK CoQuS W1210), the Austrian Nano Initiative project (PLATON), and the Austrian Society for Microelectronics (GMe).

[1]J. Faist, F. Capasso, D. L. Sivco, C. Sirtori, A. L. Hutchinson, and A. Y. Cho, Science **264**, 553 (1994).
[2]Y. Yao, A. J. Hoffman, and C. F. Gmachl, Nat. Photonics **6**, 432 (2012).
[3]S. Kumar, IEEE J. Quantum Electron. **17**, 38 (2011).

[4]Y. Bai, N. Bandyopadhyay, S. Tsao, S. Slivken, and M. Razeghi, Appl. Phys. Lett. **98**, 181102 (2011).
[5]S. Fathololoumi, E. Dupont, C. W. I. Chan, Z. R. Wasilewski, S. R. Laframboise, D. Ban, A. Mátyás, C. Jirauschek, Q. Hu, and H. C. Liu, Opt. Express **20**, 3866 (2012).
[6]B. S. Willliams, S. Kumar, Q. Hu, and J. L. Reno, Electron. Lett. **42**, 89 (2006).
[7]E. Benveniste, A. Vasanelli, A. Delteil, J. Devenson, R. Teissier, A. Baranov, A. M. Andrews, G. Strasser, I. Sagnes, and C. Sirtori, Appl. Phys. Lett. **93**, 131108 (2008).
[8]L. Ajili, G. Scalari, N. Hoyler, M. Giovannini, and J. Faist, Appl. Phys. Lett. **87**, 141107 (2005).
[9]M. Fischer, G. Scalari, K. Celebi, M. Amanti, Ch. Walther, M. Beck, and J. Faist, Appl. Phys. Lett. **97**, 221114 (2010).
[10]K. Fujita, M. Yamanishi, S. Furuta, K. Tanaka, T. Edamura, T. Kubis, and G. Klimeck, Opt. Express **20**, 20647 (2012).
[11]A. Bismuto, S. Riedi, B. Hinkov, M. Beck, and J. Faist, Semicond. Sci. Technol. **27**, 045013 (2012).
[12]N. Bandyopadhyay, S. Slivken, Y. Bai, and M. Razeghi, Appl. Phys. Lett. **100**, 212104 (2012).
[13]C. Deutsch, A. Benz, H. Detz, P. Klang, M. Nobile, A. M. Andrews, W. Schrenk, T. Kubis, P. Vogl, G. Strasser, and K. Unterrainer, Appl. Phys. Lett. **97**, 261110 (2010).
[14]M. I. Amanti, G. Scalari, R. Terazzi, M. Fischer, M. Beck, J. Faist, A. Rudra, P. Gallo, and E. Kapon, New J. Phys. **11**, 125022 (2009).
[15]M. Nobile, P. Klang, E. Mujagić, H. Detz, A. M. Andrews, W. Schrenk, and G. Strasser, Electron. Lett. **45**, 1031 (2009).
[16]S. Kumar, Q. Hu, and J. L. Reno, Appl. Phys. Lett. **94**, 131105 (2009).
[17]J. R. Söderström, E. R. Brown, C. D. Parker, L. J. Mahoney, J. Y. Yao, T. G. Andersson, and T. C. McGill, Appl. Phys. Lett. **58**, 275 (1991).
[18]C. Deutsch, H. Detz, T. Zederbauer, A. M. Andrews, P. Klang, T. Kubis, G. Klimeck, M. E. Schuster, W. Schrenk, G. Strasser, and K. Unterrainer (unpublished).
[19]R. M. Feenstra, D. A. Collins, D. Z.-Y. Ting, M. W. Wang, and T. C. McGill, Phys. Rev. Lett. **72**, 2749 (1994).
[20]J. B. Khurgin, Appl. Phys. Lett. **93**, 091104 (2008).
[21]M. A. Belkin, J. A. Fan, S. Hormoz, F. Capasso, S. P. Khanna, M. Lachab, A. G. Davies, and E. H. Linfield, Opt. Express **16**, 3242 (2008).
[22]D. Turčinková, G. Scalari, F. Castellano, M. I. Amanti, M. Beck, and J. Faist, Appl. Phys. Lett. **99**, 191104 (2011).